Preprints of the 18th IFAC World Congress
Milano (Italy) August 28 - September 2, 2011

Robotic burrowing in brain parenchyma tissue

Gabor Kosa*, Danilo De Lorenzo,
Elena De Momi**, Gabor Szekely***, Giancarlo Ferrigno****

*Robots and BioMedical Micro Systems, School of Mechanical Engineering, Tel Aviv University (Tel: +972-4-6408788; email: gkosa@post.tau.ac.il).
**NearLab, Biongineering Department, Politecnico di Milano (Tel: +39-02-2399-9013; e-mail: danilo.delorenzo@mail.polimi.it, elena.demomi@polimi.it, giancarlo.ferrigno@polimi.it).).
***Computer Vision Laboratory, D-ITET, ETH Zurich (Tel: +41-44-6325288; email: szekely@vision.ee.ethz.ch).

Abstract: Several brain pathologies could take advantage of local delivery of drugs or electrical stimulation for the treatment of tumors or neurological disorders. A self propelling microdevice could reach remote locations and is available for further precision positioning in time, also after months. In this paper we present a study for the locomotion of such a micro-device. The proposed device is built of piezoelectric actuators that create an undulating motion which is capable of propelling the micro-robot in the brain parenchyma. In order to estimate the feasibility of such device we measured the resonant frequencies of an up-scaled actuator in air and brain tissue mimicking gel and found that it can actually burrow into the tissue. An optimally designed actuator is able to produce a maximal propulsive velocity of 25 mm/s and propulsive force of 8.7 mN. Relying on a realistic power consumption of 10 mW will reduce the performance to 1 mm/s and 0.34 mN.

1. INTRODUCTION

The future of brain tumour treatment is the possibility to release highly toxic molecules with pinpoint accuracy. Deep Brain Stimulation (DBS) can ease the symptoms of different neurological diseases such as Parkinson, dystonia or essential tremor (Liker et al., 2008). One difficulty in DBS is the loss of the effectiveness of the treatment due to electrode migration. One of the solutions is to change the location of the electrode, moving the electrode from outside. Their external displacement is difficult hence we suggest a burrowing mechanism that will enable the migration of the electrode to new target cells through a controlled carrier. Such a solution would also support the local delivery of drugs for tumour treatment or epilepsy control.

Various actuators have been suggested for the locomotion of micro robots. Catheters can place the micro-systems using external force (Frasson et al., 2007). Various swimming methods have been suggested using magnetic (Zhang et al., 2009; Yesin et al., 2006; Ishiyama et al., 2001), piezoelectric (Kosa et al., 2007, Watson et al., 2009) and electro active polymer (Guo et al., 2006) actuators. They work in water or other fluids.

The only microsystem that successfully demonstrated untethered movement in tissue is a 12XØ2 mm magnetic drill-like micro robot (Ishiyama et al., 2001), that can run trough bovine tissue at 1 mm/s. The robot also successfully demonstrated motion in a wide range of gels.

Although there is vast literature on the swimming of micro-organisms in a viscous fluid (Cohen and Boyle, 2009) not many studies consider swimming in a viscoelastic media. Fulford et al. (Fulford et al., 1998) expanded the resistive force theory, originated by Gray and Hancock (Gray and Hancock, 1955), taking into consideration the properties of a linear viscoelastic fluid. Fulford found that, in a first order approximation, swimming in viscoelastic fluid and Newtonian fluid is the same. Later a more generic model handling a waving sheet's swimming was developed by Lauga (Lauga, 2007).

We suggest to use the swimming method developed in (Kosa et al., 2007) to propel a micro-system in the brain parenchyma. In order to design such a robot one needs to evaluate the viscoelastic properties of the brain tissue. Hrapko et al. (Hrapko et al., 2008) showed that there's a lot of inconsistency on brain properties in literature. The ranges for shear stress and loss moduli vary depending on temperature, material anisotropy, post-mortem time and the chosen amount of pre-compression in shear measurements. Differences are in the range of one order of magnitude. Recently, magnetic resonance elastography allowed deriving viscoelastic properties of the brain under in-vivo conditions. However, different and partially contradicting results were reported (Sack et al., 2009). Also, there is lack of detailed information of the brain tissue behaviour at high frequencies (above 1kHz). Given this data, it becomes a challenge understanding which parameters to use in order to simulate the performances of the swimming micro-robot.
Gelatine is the mostly used material to mimic soft tissue behaviour. It is easy to prepare it and to control its mechanical properties varying the percentage in water. Therefore, gelatine is a good material for obtaining preliminary results on the burrowing properties of such a microrobot. Even if the gelatine properties are well known at low frequencies, there is only one paper describing viscoelastic behaviour of gelatine at high frequencies

(Salisbury and Cronin, 2009). By using these results we extracted the viscoelastic parameters of the gelatine assuming a Maxwell model and running the simulation of the experiment detailed in the Salisbury article (Salisbury and Cronin, 2009). In this paper, preliminary evaluation of the commercial actuator's ability to advance in the measured materials is shown and the performances of a microsystem that can be embedded in the brain is evaluated.
In (Kosa et al., 2007) the swimming ability of a microrobot in a highly viscous liquid is reported. Although the model does not take into account the elastic aspect of the viscoelastic media we use it to evaluate the amplitude of the travelling wave that can be created in the gel.
Using our proposed micro robot will enable the positioning of the electrode's tip in the brain. Because of the small size of the micro robot, the small amplitude of the travelling wave (15-75 µm) and the high travelling wave velocity (travelling wave velocity: U=50-100 m/s; the advance velocity of the whole device is $U^{(0)}$=1-10 mm/s) in the actuators, we estimate that the damage to the brain parenchyma will be minimal. Studies show that increasing the relative velocity between the tissue and the penetrating object reduces the tissues reacting force e.g. the tissue damage (Mahvash and Dupont, 2009).

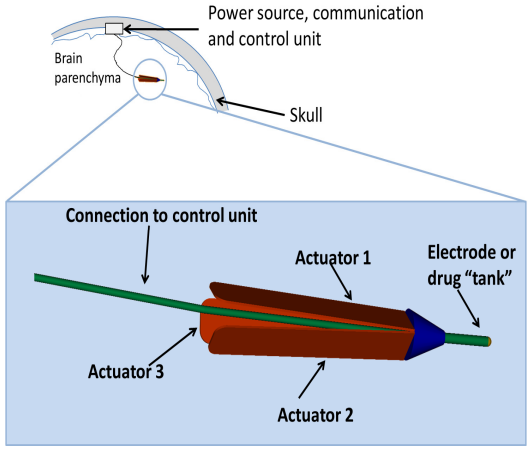

Fig. 1. Illustrative drawing of the propulsion of the burrowing micro robot.

2. MATERIALS AND METHODS

2.1 Micro-robot design

The target design of the robot will have three piezoelectric tails, as shown in Fig. 1, which will enable manoeuvring in 5 Degrees of Freedom (DoFs). In the brain parenchyma we will place only the actuators for positioning and the other parts (power source, command and control unit, communication transceiver) of the robot will remain under the patient skull. The overall size of the robot's head is 12 mm X Ø3mm.
The medical task's geometrical constraints limit the length and the width of the actuator to 11mm and 2.5mm. The overall thickness of the actuator should be 0.1 mm so that the propelling device will not be too brittle.
The swimming tails are clamped to top part of the device (blue cap in Fig. 1) and placed symmetrically. Such a setup prevents the wiggling of the head and creates forward propulsion with ability to turn the head orthogonal to its line of symmetry.

2.2 APC bimorph piezoelectric bending actuator

As a preliminary study, we examined the performance of a single tail that can move along its insertion line into the brain. The APC-40-1055 stripe actuator (Catalog No. 40-1055 (350/025/0.60-SA) manufactured by American Piezo Ceramics Ltd. From here and on APC) has a total length of 35 mm, a width of 2.5mm and a thickness of 0.6 mm. The actuator has two 200µm thick PZT layers, with a very thin electrode on each side and middle layer of 180µm unknown material. The electrodes and covering layers overall thickness is 20µm.The APC actuator is built by bulk single layer technology. In order to evaluate the suggested locomotion method's true potential we designed an actuator that has different dimension and manufacturing technology from the APC.

2.3 Multilayer actuator

More advanced piezoelectric actuators such as the bending actuators manufactured by the Noliac group (Noliac, 2010) are made with multilayer technology that enables manufacturing thinner devices using lower driving voltages. The co-fired multi-layer actuators have a maximal electrical field of 3000V/mm therefore the maximal driving voltage of a 20µm layer is 60 Volt.

2.4 Experimental Protocol

In order to estimate the resonant frequencies (at the different vibration modes) of the APC strip actuator we clamped it by its base electrode (31mm length) and measured the resonant frequencies in air and in the gelatine (Fig.2). The gelatine sample was prepared with a 10% concentration in pure water at 4°C. Since the APC stripe actuator is made by two PZT layers we excited only one layer and we used the second layer as a sensor in order to acquire the response of the actuator (Fig.3). The element was driven with a sinusoidal sweep with a frequency up to 20kHz at 24V. The signal was acquired using the USB-6009 DAQ board by National Instrument and in correspondence of the maximum amplitude of the signal (resonant frequency) the frequency was computed as the inverse of the sinusoid period.

2.5 Boundary conditions

To obtain the right boundary conditions, we calculated the elastic constant and the viscosity of the gelatine running a simulation to match the data shown in (Salisbury and Cronin, 2009) using a linear Maxwell model, for 20% and 10% gelatine concentration. A simulation was run to fit the data for all the frequencies shown in (Salisbury and Cronin, 2009) (from 350Hz up to 4000Hz), focusing on the measured resonant frequencies of the stripe actuator, i.e. 1250Hz and 3250Hz.
In the simulation, we computed the step response of the Maxwell model simulating the stress relaxation experiment for each frequency. Then the stress-strain response was computed changing the Maxwell model parameters (the elastic modulus E and the viscosity η, Fig. 4) according to:

$$\sigma = \varepsilon \cdot e^{-\left(\frac{g}{\eta} \cdot t\right)} \quad (1)$$

where σ is the stress, ε the strain, and t the time.

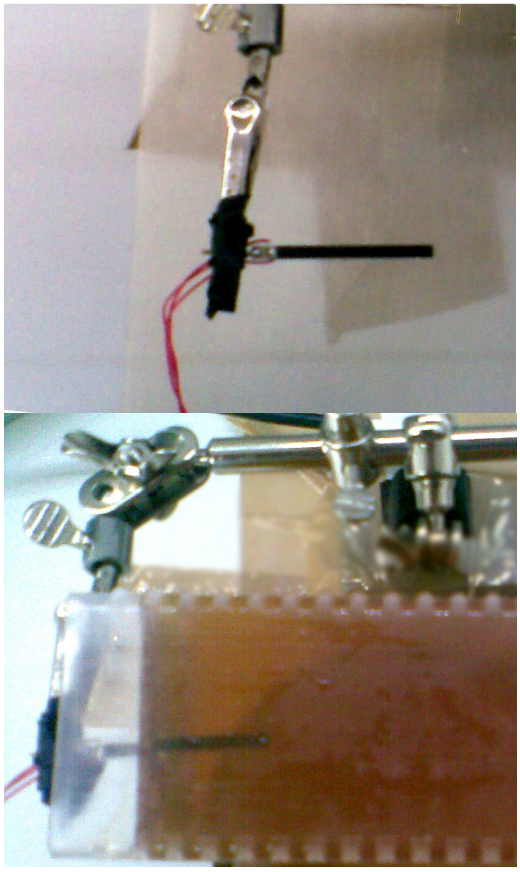

Fig. 2. Experimental setup for the resonant frequency assessment of the strip actuator in air (top) and in gelatine (bottom).

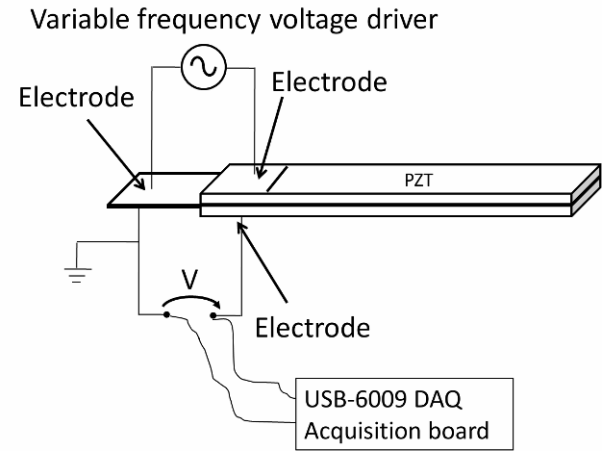

Fig. 3. Illustrative drawing of the experimental setup for the resonant frequency computation.

The best matching E and η were found minimizing the square of the difference between the curve fitting the experimental data shown in the Salisbury paper (Salisbury and Cronin, 2009) and the simulated Maxwell data for each frequency:

$$\min\left\{\left(\sigma_{\exp}-\sigma_{Maxwell}\right)^2\right\} \quad (2)$$

where σ_{exp} is the true stress on the experimental data from Salisbury and Cronin (Salisbury and Cronin, 2009) and $\sigma_{Maxwell}$ the true stress of the simulated data with the Maxwell model.

Fig. 4. Maxwell model.

2.5 Travelling wave amplitude and frequency estimation

We matched the first three measured resonant frequencies by changing the middle layers stiffness and changing the stiffness of the boundary condition.

Using the stiffness and boundary conditions calibrated by the resonant frequencies, we estimated the frequency, wavelength and amplitude of the travelling wave that can be created with the stripe actuator. The travelling wave's description is

$$w(x,t)=b\sin\kappa(x+Ut) \quad (3)$$

where $w(x,t)$ is a sinusoidal undulating beat or a travelling wave. b, $\kappa=2\pi/\lambda$, $\omega=2\pi f=\kappa U$ are the amplitude, wave number and frequency of the travelling wave. λ is the wavelength, f is the frequency and U is the velocity of the travelling wave advancing in the tail.

In (Kosa et al., 2007) we found that the closest approximation to a travelling wave is when $\lambda=L$ (L is the length of the actuator) and that the swimming tail is most effective when the excitation frequency is equal to the third resonant frequency of the beam, $f=f_3$.

2.6 Stripe actuator motion simulation

The motion of the actuator is characterized by the swimming velocity ($U^{(0)}$) and propulsive force (F_p). The maximal swimming velocity is achieved when the drag force of the swimming tail moving at velocity U is balanced by propulsive force F_p. The propulsive force F_p is fully applied on the tissue when U is zeroed and the actuator applies the undulating motion on the tissue. According to (Fulford et al., 1998)

$$U^{(0)}=\frac{\omega}{\kappa}\frac{\beta_0^2}{2}\frac{1-r}{r+(2-r)\beta_0^2/4}+O(\beta_0^4) \quad (4)$$

.

$$F_P=\frac{\omega\kappa b^2 LC_N^{(0)}(1-r)}{2}.$$

where $\beta_0=2\pi b/\lambda$ is the non-dimensional ratio between the amplitude and the wavelength of the travelling wave. $r=C_T^{(0)}/C_N^{(0)}$ is the ratio between the tangential $C_T^{(0)}$ and normal $C_N^{(0)}$ resistance coefficients as defined in (Gray and Hancock, 1955).

$$C_N^{(0)} = \frac{4\pi\eta^{(0)}}{\log\left(\frac{2\pi r_0}{L}\right) - \frac{1}{2}} \qquad (5)$$

$$r = \frac{1}{2}\frac{\ln 2 + \ln \pi + \ln(r_0 / L) + 1/2}{\ln 2 + \ln \pi + \ln(r_0 / L) - 1/2}$$

where r_0 is the equivalent radius derived from the rectangular shape function's Fourier decomposition of the actuator. The value of this radius for a 0.6 mmX2.5 mm rectangular cross section is $r_0 = 0.6[mm]$. $\eta^{(0)}$ is the lowest order of the damping coefficient's decomposition (Fulford et al., 1998). In the case of a linear Maxwell model viscoelastic material, $\eta^{(0)}$ is the zero shear rate damping coefficient and its value is $\eta^{(0)} = 14.32[Pa \cdot s]$ for the 20% gelatine at 3200Hz (Table 1A).

3. RESULTS

Table 1A and Table 1B show the values of *E* and η for the 10% and 20% gelatine at different frequencies, while Fig. 5 shows the experimental data from (Salisbury and Cronin, 2009) and the simulated one at 3250Hz. Fig. 5 also shows the elastic modulus with respect to the frequency for the 20% gelatine.

Table 1A. Maxwell model – elastic modulus and viscosity of the 20% gelatine 10°C

Frequency [Hz]	*E(MPa)*	η (Pas)
350	0.1620	6.0359
400	0.3734	23.33
750	1.057	46.62
1350	1.26	33.26
3200	3.099	14.32
4000	8.063	11.01

Table 1B. Maxwell model – elastic modulus and viscosity of the 10% gelatine 10°C

Frequency [Hz]	*E(MPa)*	η (Pas)
1000	0.23	11.87
1250	0.20	13.16
1550	0.47	8.34

Table 2 shows the resonant frequencies of the actuator, obtained experimentally and analytically from a semi-clamped (clamped by stiff springs) Euler-Bernoulli cantilever model. The motion in gel adds considerable damping and reduces the resonant frequencies due the additional stiffness and damping added to the beam from the mechanical response of the gelatine.

Using the stiffness and boundary conditions calibrated by the resonance frequencies, the values for the APC #40–1055 travelling wave's wavelength, frequency and velocity estimations are:

$$\lambda = L = 31 \cdot 10^{-3}[m],\ f = f_3 = 3384\,[Hz] \Rightarrow U = \lambda f = 104.9[m/s] \qquad (6)$$

Using the parameters (6) and the proper viscosity, $\mu(\omega) = 14.32[Pa \cdot s]$ (Table 1A), we estimated the amplitude of the travelling wave along the swimming tail. The actuator's driving voltages are:

$$\varphi_i(t) = 75 + 75\sin(21261\,t + \phi_i)\ [V] \qquad \forall i = 1..3 \qquad (7)$$

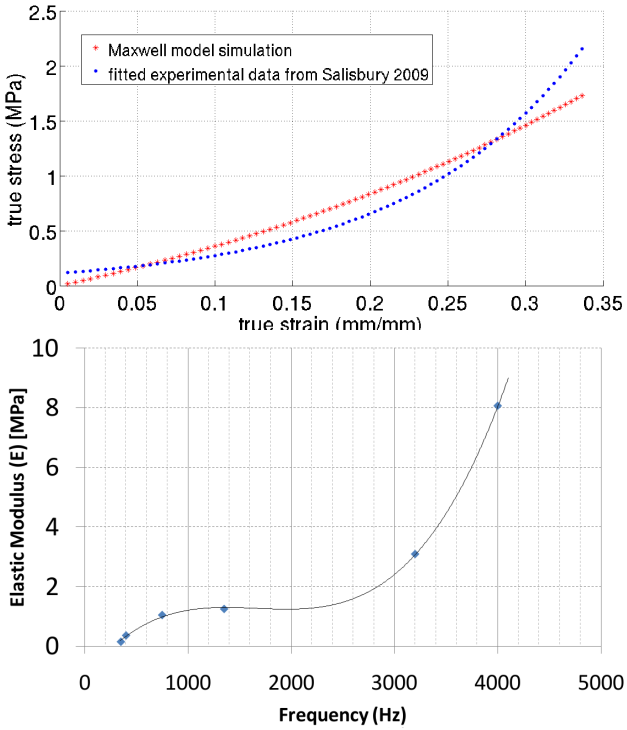

Fig. 5. – Example of simulated true-stress/true-strain curves and experimental curves from (Salisbury and Cronin, 2009) for 3250Hz (top) and elastic moduli with respect to frequency for each simulated frequency (bottom).

Table 2. Resonant frequencies of the APC actuator

Frequency [Hz]	Theory in Air	Experiment in Air	Experiment in Gel
f_1	155	155	-
f_2	1170	1118 1158 1222	1100 1282
f_3	3514	3384	3142

(ϕ_i are the phases legs that are needed to create the travelling wave in the different sections of the actuator, (see (Kosa et al., 2007) for details) in the direction of the polarization. The approximated travelling wave is:

$$w(x,t) = 15.5\sin 202\,(x + 104.9t)\ [\mu m] \qquad (8)$$

The advancing velocity of the APC #40–1055 swimming actuator according to the (Fulford et al., 1998) approach without additional added external load or head section is therefore:

$$U_{APC}^{(0)} = 1.2[mm/s] \quad (9)$$

and the propulsive force is:

$$F_P = 1.28[mN] \quad (10)$$

The advancement velocity is therefore more than sufficient for burrowing in the brain.

Table 3. Resonant frequencies of the multilayer actuator

Frequency [Hz]	Calculated for Gel
f_1	50
f_2	1667
f_3	5386

Table 3 shows the computed resonance frequencies of the multilayer actuator. Using this data, the travelling wave results:

$$w(x,t) = 72.2 \sin 571.2(x + 59.25\, t)\ [\mu m]. \quad (11)$$

As a result the swimming velocity and propulsive force will be:

$$U_{MLA}^{(0)} = 25.6[mm/s] \text{ and } F_P = 8.7[mN]. \quad (12)$$

The power consumption of the actuator is 1.068W which is difficult to supply by existing micro power sources.
A more realistic propulsion mode is limiting the input power to 10.7mW and maintaining a locomotion velocity of 1 mm/s with a propulsive force of 0.34mN**.**

4. CONCLUSIONS

The results showed that the elastic modulus of the gelatine increases with the frequency, particularly over 3kHz. The viscosity range is between 6 and 46 $Pa{\cdot}s$, and it is not always increasing with frequency. This result is due to the dominant elastic behaviour for such high frequencies so that small changes in the η parameter do not affect the results for the Maxwell-model approximation. Further investigation will be performed using different viscoelastic models such as Voigt and spring-spot models.
We showed in this paper that burrowing into the brain tissue by a piezoelectric propulsive micro-device is feasible and realistic, since the computed force and velocity values are within the ranges of the specific surgical task. In the future we intend to perform additional experiments using gelatine and brain tissue at high frequencies in order to validate the theoretical results presented above.

REFERENCES

Cohen N and Boyle JH. (2009) Swimming at low Reynolds number: a beginners guide to undulatory locomotion. *Contemporary Physics* 51: 103 - 123.

Frasson L, Ko SY, Turner A, et al. (2007) STING: a soft-tissue intervention and neurosurgical guide to access deep brain lesions through curved trajectories. *Proceedings of the Institution of Mechanical Engineers, Part H: Journal of Engineering in Medicine* 224: 775-788.

Fulford GR, Katz DF and Powell RL. (1998) Swimming of spermatozoa in a linear viscoelastic fluid. *Biorheology* 35: 295-309.

Gray J and Hancock GJ. (1955) The Propulsion of Sea-Urchin Spermatozoa. *J Exp Biol* 32: 802-814.

Guo SX, Ge YM, Li LF, et al. (2006) Underwater swimming micro robot using IPMC actuator. *IEEE ICMA 2006: Proceeding of the 2006 IEEE International Conference on Mechatronics and Automation, Vols 1-3, Proceedings*: 249-254.

Hrapko M, Dommelen JAWv, Peters GWM, et al. (2008) The Influence of Test Conditions on Characterization of the Mechanical Properties of Brain Tissue. *Journal of Biomechanical Engineering* 130: 031003.

Ishiyama K, Sendoh M, Yamazaki A, et al. (2001) Swimming micro-machine driven by magnetic torque. *Sensors and Actuators A: Physical* 91: 141-144.

Kosa G, Shoham M and Zaaroor M. (2007) Propulsion method for swimming microrobots. *IEEE Tansactions on Robotics* 23: 137-150.

Lauga E. (2007) Propulsion in a viscoelastic fluid. *Physics of Fluids* 19: 083104.

Liker MA, Won DS, Rao VY, et al. (2008) Deep Brain Stimulation: An Evolving Technology. *Proceedings of the IEEE* 96: 1129-1141.

Mahvash M and Dupont PE. (2009) Fast needle insertion to minimize tissue deformation and damage. *Robotics and Automation, 2009. ICRA '09. IEEE International Conference on.* 3097-3102.

Noliac. (2010) www.noliac.com. Available at: http://www.noliac.com/.

Sack I, Beierbach B, Wuerfel J, et al. (2009) The impact of aging and gender on brain viscoelasticity. *Neuroimage* 46: 652-657.

Salisbury CP and Cronin DS. (2009) *Mechanical Properties of Ballistic Gelatin at High Deformation Rates,* Heidelberg, ALLEMAGNE: Springer.

Yesin KB, Vollmers K and Nelson BJ. (2006) Modeling and Control of Untethered Biomicrorobots in a Fluidic Environment Using Electromagnetic Fields. *Int. J. Rob. Res.* 25: 527-536.

Zhang L, Abbott JJ, Dong L, et al. (2009) Characterizing the Swimming Properties of Artificial Bacterial Flagella. *Nano Letters* 9: 3663-3667.